A Pilot Study of Quantitative MRI Parametric Response Mapping of Bone Marrow Fat for Treatment Assessment in Myelofibrosis

Gary D. Luker[1,2,3], Huong (Marie) Nguyen[4], Benjamin A. Hoff[1], Craig J. Galbán[1], Diego Hernando[5], Thomas L. Chenevert[1], Moshe Talpaz[4], and Brian D. Ross[1,6]

[1]Center for Molecular Imaging, Department of Radiology, and [2]Departments of Biomedical Engineering and [3]Microbiology and Immunology, University of Michigan, Ann Arbor, Michigan; [4]Department of Internal Medicine, Division of Hematology/Oncology, University of Michigan, Ann Arbor, Michigan; [5]Department of Radiology, University of Wisconsin-Madison, Madison, Wisconsin; and [6]Department of Biological Chemistry, University of Michigan, Ann Arbor, Michigan

Corresponding Authors:
Brian D. Ross
University of Michigan Center for Molecular Imaging, 109 Zina Pitcher Place, 2071 BSRB, Ann Arbor, MI 48109-2200
E-mail: bdross@umich.edu; and Moshe Talpaz,
E-mail: mtalpaz@med.umich.edu

Key Words: magnetic resonance imaging, bone marrow, myelofibrosis, ruxolitinib
Abbreviations: Myelofibrosis (MF), magnetic resonance imaging (MRI), polycythemia vera (PV), essential thrombocytosis (ET), Dynamic International Prognostic Scoring System Plus (DIPSS Plus), bone marrow fat fraction (FF), parametric response mapping (PRM), volumes of interest (VOI)

ABSTRACT

Myelofibrosis (MF) is a hematologic neoplasm arising as a primary disease or secondary to other blood malignancies. Both primary and secondary MF develop progressive fibrosis of bone marrow, displacing normal hematopoietic cells to other organs and disrupting normal production of mature blood cells. Activation of JAK2 signaling in hematopoietic stem cells commonly causes MF, and ruxolitinib, a drug targeting this pathway, is the preferred treatment for many patients. However, current measures of disease status in MF do not necessarily predict response to treatment with ruxolitinib or other drugs. Bone marrow biopsies are invasive and prone to sampling error, while measurements of spleen volume only indirectly reflect status of bone marrow. Toward the goal of developing an imaging biomarker for treatment response in MF, we present preliminary results from a prospective clinical study evaluating parametric response mapping (PRM) of quantitative Dixon MRI bone marrow fat fraction maps in four MF patients treated with ruxolitinib. PRM allows voxel-wise identification of temporal changes in quantitative imaging readouts, in this case bone marrow fat. We identified heterogeneous responses of bone marrow fat among patients and within different bone marrow sites in the same patient. Changes in bone marrow fat fraction also were discordant with reductions in spleen volume, the standard imaging metric for treatment response. This study provides initial support for PRM analysis of quantitative MRI of bone marrow fat to monitor therapy in MF, setting the stage for larger studies to further develop and validate this method as a complementary imaging biomarker.

INTRODUCTION

Myelofibrosis (MF) is a myeloproliferative neoplasm caused by unregulated proliferation of abnormal hematopoietic stem cells, resulting in progressive fibrosis of the bone marrow. MF may occur as a primary disease or develop secondary to polycythemia vera (PV) or essential thrombocythemia (ET). Patients with MF can have hyperproliferation or underproduction of blood cells (polycythemia or anemia), reduced or elevated white blood cell counts (leukopenia or leukocytosis), and reduced or elevated platelet counts (thrombocytopenia or thrombocytosis) (1). The shift of hematopoiesis away from the fibrotic bone marrow to other anatomic sites, referred to as extramedullary hematopoiesis, produces profound hepatosplenomegaly. Patients also experience debilitating constitutional symptoms such as fever, night sweats, myalgias, and weight loss because of the release of proinflammatory cytokines. Even with the state-of-the-art drugs, less than half of the patients exhibit durable responses to treatment, and the median survival rate ranges from ~2–17 years (2). As an additional complication, 8%–20% of patients with MF progress to acute myeloid leukemia (3).

Although many inciting events causing MF remain unknown, an activating mutation in *JAK2* (V617F) occurs in 50%–60% of patients with primary MF/ET and >95% of those with PV (4). Discovery of *JAK2* V716F led to the development of JAK2 inhibitors with the U.S. Food and Drug Administration approval for ruxolitinib in 2011, which, now, is the drug of choice for many patients with MF (5). Treatment with ruxolitinib reduces the spleen size and improves constitutional symptoms (6). Even in patients with MF without the *JAK2* V716F mutation, treatment with ruxolitinib also improves survival (7).

ISSN 2379-1381 http://dx.doi.org/10.18383/j.tom.2016.00115

Despite the overall benefits of ruxolitinib, few patients experience either partial or complete responses (eg, reversion of bone marrow fibrosis or leukoerythroblastosis or peripheral blood count normalization). Disease symptoms can also recur within 7–10 days of discontinuing ruxolitinib. Some patients treated with JAK2 inhibitors exhibit a phenomenon called "disease persistence," defined as the gradual return of splenomegaly and constitutional symptoms despite continued JAK2 inhibitor treatment (8). The inability to distinguish patients who maintain durable responses to ruxolitinib and ultimately show at least partial regression of bone marrow fibrosis from those who exhibit disease persistence remains a major clinical challenge.

Patients with MF are classified into 4 risk groups based on the Dynamic International Prognostic Scoring System Plus (DIPSS Plus). DIPSS Plus stratifies patients based on the following criteria: age >65 years, hemoglobin level <10, white blood count >25 000, platelet count <100 000, and circulating blast percentage ≥1%; presence of constitutional symptoms; unfavorable cytogenetics; and red cell transfusion dependence (9). One point is assigned to each DIPSS Plus criterion, with higher scores associated with decreased survival. However, DIPSS Plus stages overall survival and does not predict response to treatment.

Bone marrow fibrosis in MF is assessed by biopsy of a single site in the iliac crest. The degree of marrow fibrosis is determined using the European Consensus criteria, which grade bone marrow fibrosis at 4 levels, from MF-0 (prefibrotic) to MF-3 (densely fibrotic) (10). In a recent study, a combination of fibrosis grade and DIPSS Plus score seems to provide general prognostic information. Low-to-nonexistent fibrosis (MF-0) in combination with low-risk DIPSS Plus correlates with good prognosis, whereas MF-3 in combination with high-risk DIPSS Plus has worse prognosis (11). The relationship among fibrosis, DIPSS Plus risk group, and outcomes supports the rationale that a significant degree of fibrosis correlates with worsened survival, although these parameters have not been used to predict treatment responses. Unfortunately, many higher-risk patients are already at either MF-2 or MF-3 fibrosis at the time of diagnosis, which highlights a notable limitation of the fibrosis grading criteria for clinical management. Once fibrosis has reached MF-3 in a biopsy sample, one cannot differentiate further worsening of fibrosis by grading. Furthermore, pathological analysis of the bone marrow from biopsy of a single site in the iliac crest currently is used as the standard for assessing the extent of fibrosis throughout all bone marrow and disease progression/regression in response to treatment. This method can be prone to misrepresentation in cases with heterogeneously distributed disease. Additional methods are needed to distinguish between patients without any or only brief responses to treatment and those with sustained benefits from therapy, as it pertains to the evaluation of fibrosis and the bone marrow niche.

As an initial step toward establishing an imaging method to more globally monitor effects of therapy on the bone marrow environment in MF, we used magnetic resonance imaging (MRI) with quantitative determination of bone marrow fat fraction (FF). We focused on this noninvasive MRI technique because the bone marrow fat content progressively increases with aging, reaching approximately 50%–70% in patients older than 50 years (12). This age group encompasses the patient population (50–70 years) predominantly affected by MF. Changes in the bone marrow associated with MF, such as replacement of the bone marrow fat by fibrosis or elevated numbers of hematopoietic cells, reduce the abundance of fat. We hypothesized that MRI could detect changes in the bone marrow fat over the course of therapy with ruxolitinib.

Spatial heterogeneity in disease and therapeutic response represents a major confounding factor to the evaluation of quantitative imaging results. To improve our ability to define spatial and temporal changes in the bone marrow fat during treatment, we used parametric response mapping (PRM), an image analysis technique we developed to identify significant changes in a quantitative imaging parameter such as FF (PRM_{FF}) on a voxel-wise basis between pre- and post-treatment image acquisitions (13). Because response is evaluated on a voxel-by-voxel basis, the PRM results are less susceptible to volume-averaging effects. PRM has shown greater sensitivity than whole-volume statistics (ie, mean) for determining heterogeneous treatment response in cancer (13-16), and it provides a spatial context for response readouts, which, in this case, may help to match the pathology results with imaging metrics. Here, we report the results of PRM_{FF} for 4 patients with MF treated with the JAK2 inhibitor, ruxolitinib. We also compared results with changes in spleen volume by MRI, which has been used as the primary endpoint for determining treatment response to ruxolitinib (5). PRM_{FF} highlighted the major regions of significant increase in FF (PRM_{FF+}), as well as substantial spatial heterogeneity in therapeutic response. Interestingly, the PRM results for FF in these 4 patients were discordant with the clinical standard of changes in spleen volume. Although further investigation is needed to define the clinical implications of PRM_{FF+} in MF, these preliminary results establish the feasibility of quantifying changes in the bone marrow fat during therapy and potential promise as a complementary approach for determining treatment efficacy.

METHODS

Patients

Patients with biopsy-proven MF beginning therapy with ruxolitinib were eligible for this single-site study. Patients with contraindication to MRI and/or needing sedation or anesthesia to undergo MRI were excluded. All participants signed the informed consent for the study, which was approved by the University of Michigan Institutional Review Board.

Study Procedures

Enrolled patients underwent MRI within 1 month before starting treatment with ruxolitinib. The ruxolitinib dose was determined by the treating hematologist and was not specified in the protocol. However, patients received between 20 and 40 mg of drug daily. Patients underwent repeat MRI studies after ~1–2, 3–5, and 6–10 months of ruxolitinib treatment for a total of 4 scans per patient.

MRI Methods for Quantitative FF and Spleen Volume

Quantitative proton density FF MRI examinations were performed on a commercial 3 T MRI system (Ingenia model, soft-

ware version 5.1.7.0; Philips Healthcare, Best, The Netherlands) using a multiecho Dixon technique (17). For each section, six complex-valued gradient echo images were acquired at echo times TE (n) = 1.23 milliseconds + 0.98 milliseconds × n (where n = 0, 1, 2, . . . 5). These images were automatically processed on the scanner to produce "water-only," "fat-only," "in-phase," "out-of-phase," "fat-fraction," and "T2*" maps of each imaged section. On-line processing included correction for magnetic field inhomogeneity, multiple peaks in the lipid spectrum, and T2* decay. In addition, a low flip-angle (nominal 3°) was used to mitigate T1 weighting, which inflates the FF values, thereby achieving proton density-weighted FF estimates at the pixel level (18). Acquisition geometry was tailored to cover patient anatomy in the lumbar and pelvis zones in 2 distinct sections. The following are the other relevant acquisition settings of the Dixon technique: a 28-channel torso receiver coil placed on abdomen/pelvis; dual-channel transmit for patient-specific "B1-shimming"; 3-dimensional (3D) fast field echo acquired with parallel imaging acceleration (SENSE = 2) in the anterior–posterior direction; repetition time (TR) is 7.5 milliseconds; field of view (FOV) is 400 × 400 mm; and acquired section thickness is 3.5 mm reconstructed to 1.75 mm for coverage of 110–147 sections at nominal 1.67- × 1.67-mm in-plane resolution.

To quantify spleen volumes, we used a 3D axial THRIVE sequence with breath-hold. The following are the sequence parameters: TE = 1.3 milliseconds, TR = 2.8 milliseconds, FOV = 400 × 400 × 16 mm, flip-angle = 10°, and excitation for a section thickness of 5 mm = 1.

FF Validation Phantom

Image acquisition of a fat/water MRI phantom (19, 20) consisting of tubes with varying fat content was performed on the clinical scanner to assess the accuracy of our FF results. Expected FFs for this phantom were 0, 2.6, 5.3, 7.9, 10.5, 15.7, 20.9, 31.2, 41.3, 51.4, and 100%. A volume of interest (VOI) was contoured within each phantom tube data set and used to generate imaging statistics for comparison with expected values using the Bland–Altman plot.

PRM of Bone Marrow FF. Image analysis was performed using an in-house software developed in MATLAB (The Mathworks, Inc., Natick, Massachusetts). Manual VOIs were individually delineated for each femoral head and pelvis marrow region on the baseline images. Follow-up magnetic resonance (MR) images were semiautomatically coregistered to the initial imaging time point for each separate VOI using Elastix (21). In brief, mutual information was used as a cost function in a stepwise multiresolution algorithm to optimize a rigid-body transformation between the initial and follow-up images. Only voxels within the dilated VOI were used to calculate the cost function.

A PRM threshold was determined, based on an approximation of the expected error in the FF map, to be ±10%. The resulting PRM classifications were determined by these thresholds applied to the voxel-wise difference between serial images (<130>FF = [follow-up FF] − [baseline FF]) as follows: <130>FF >10%, indicating a significant increase in FF (PRM_{FF+}, red); <−10%, indicating significant decrease in FF from the baseline (PRM_{FF-}, blue); and 0% indication no significant change (PRM_{FF0}, green). The PRM values are represented as volume fractions of each classification and are presented individually and in combination (ie, PRM_{FF+} + PRM_{FF-}).

The display of results (Figures 2–5) was facilitated by dedicated 3D visualization software (Amira, FEI, Hillsboro, Oregon), allowing for the efficient display of the masked FF maps and temporal change via PRM. For display of FF maps (left column), a color map was selected to be increasingly transparent with the decreasing fat content, and progressing from orange to yellow to white with the increasing content of fat. The PRM maps (middle column) are displayed with solid red (PRM_{FF+}), blue (PRM_{FF-}), and semitransparent green (PRM_{FF0}) to highlight regions of significant change. The PRM scatterplots (combined pelvis and femurs) are displayed in the right-hand column for additional context into the distribution of FF values.

Spleen Volumes

Spleen volumes were quantified from the pretreatment and 6-months post-treatment studies. A board-certified radiologist manually defined a region of interest around the spleen on each image and measured the areas on each section using a McKesson PACS workstation. Areas on each section were summed to obtain the total spleen volume, which was used to calculate the percent change in spleen volume between the pretreatment and final post-treatment MRI examinations.

RESULTS

Patient Population

From December 2014 through October 2015, we performed the complete study protocol of pretreatment baseline MRI with repeat examinations after approximately 1–2, 3–5, and 6–10 months of treatment on 4 patients with MF. All enrolled patients completed the study. Table 1 lists the patient characteristics. Three patients developed post-PV MF, whereas 1 patient developed post-ET MF. All patients underwent a bone marrow biopsy before therapy to establish the MF diagnosis, and patient 1 underwent a second bone marrow biopsy after completing the therapy. The pretreatment bone marrow fibrosis degree ranged from MF-1 to MF-3, based on the European Consensus criteria, which grades bone marrow fibrosis at 4 levels, from MF-0 (prefibrotic) to MF-3 (densely fibrotic). Patients 2–4 had a hypercellular bone marrow, with up to 100% cellularity on pretreatment bone marrow biopsies in patients 2 and 3. Table 1 also lists hematologic parameters for white blood cell (WBC) count, red blood cell (RBC) count, hemoglobin levels, hematocrit values, and platelet count in the peripheral blood before beginning ruxolitinib (baseline) and after the final MRI (treatment). These parameters routinely are used clinically as part of the overall assessment of bone marrow function.

MRI Phantom for Validation of FF Measurements

Overall, the image acquisition and processing methodology used in this study resulted in <4% deviation from actual FF values expected from the phantom (Figure 1). Measurements from phantom vials with low-fat content, FF values between 0% and 20%, were slightly elevated using our quantification; however, deviation of mean volume measurements from actual values did not exceed ±4%.

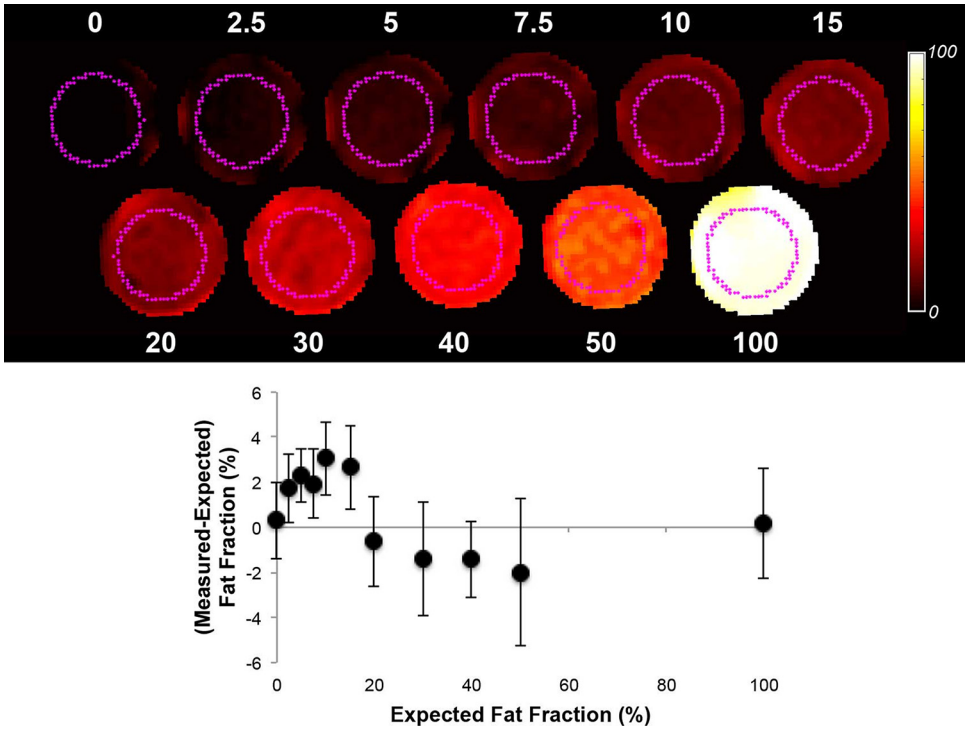

Figure 1. Calibration of fat fraction (FF) magnetic resonance imaging (MRI) with a phantom. A single axial cross-section (top) through an FF map of phantom vials, identified by approximate FF value, shows the variation of FF imaging results over a range of expected values. A mask has been applied to the FF map to zero out the voxels with no signal and focus on content of the phantom vials. The Bland–Altman analysis of phantom regions (bottom) shows good agreement between measured and expected values, with slightly elevated measurements in regions of low-fat content. Error bars represent the standard deviation within each volume of interest (VOI).

Imaging Assessment of Treatment for Individual Patients

Patient 1. Patient 1 developed post-ET MF. This patient had extensive bone marrow fibrosis (MF grade 2–3) at baseline before therapy with ruxolitinib (Table 1). On the baseline pretreatment study, the percent FF display shows ~30%–40% fat confined to each proximal femur and acetabulum (Figure 2). This percentage and distribution changed minimally after 2 months of therapy. However, the subsequent MRI examination after ~5 months demonstrated a clear increase in percent FF (60%–70%) and a broader distribution with bone marrow fat extending into both iliac bones and the superior pubic rami. The FF image at 7 months showed a comparable amount and distribution of fat as described at 4.7 months.

PRM, which quantifies the changes in percent FF on a voxelwise basis from post-treatment studies to the baseline MRI, showed a modest initial increase in the bone marrow fat in the acetabula, superior pubic rami, and femoral heads after ~2 months (Figure 2). The subsequent study at ~5 months showed marked increases in the bone marrow fat throughout the pelvis and femora, and the bone marrow fat in the iliac bones continued to increase through the 7-month examination. The PRM scatterplots for pre- versus mid-treatment FF quantitatively display the relative abundance of the bone marrow fat at baseline and reveal a significant increase in the fat throughout both the pelvis and proximal femurs at ~5 and 7 months after treatment initiation. The color display of the PRM voxels shows that treatment produced greater increases in the bone marrow fat in both femurs relative to the pelvis. Figure 2 legend contains a video link to a 3D view of spatially varying changes in the PRM values over time for patient 2.

In a marked contrast to increases in bone marrow fat, this patient had <5% reduction in spleen volume, the standard imaging metric for treatment efficacy in MF (Figure 6). These data for patient 1 display discordance between changes in bone marrow FF and spleen volume during therapy with ruxolitinib. The post-treatment bone marrow biopsy from the iliac crest showed MF grade 3 fibrosis with high numbers of megakaryocytes. In addition, a complete blood count after 7 months of therapy revealed a decrease in all parameters with below-normal values for WBC, RBC, hemoglobin, and hematocrit (Table 1).

Patient 2. Patient 2 developed post-PV MF, with the pretreatment bone marrow biopsy showing predominantly MF grade 1 fibrosis and hypercellularity (100% cellularity; Table 1). Initial MRI data showed that the bone marrow fat was essentially confined to the femoral heads bilaterally with fat content of ~50%–60% (Figure 3). Follow-up examinations at ~2 and 4 months revealed a slight expansion of the bone marrow fat restricted to the femoral heads. By comparison, the final examination at ~10 months showed a considerable increase in the bone marrow fat, extending into the iliac wings, superior pubic rami, and proximal femurs. The PRM anatomic display enhances the detection of increased bone marrow fat in both iliac wings after 2 and 4 months of treatment. However, these increases were difficult to discern on images with percent FF. The PRM also reinforces increased bone marrow fat throughout the pelvis and proximal femurs on final examination. Figure 3 legend also includes a video link that enables 3D viewing of spatially varying changes in the PRM values for patient 2 over time. Similar to patient 1, the bone marrow fat increased to a greater extent in the femurs relative to the pelvis, and patient 2 had only a limited (~10%) decrease in spleen volume that fell well below the threshold used for successful treatment (Figure 6).

Before therapy, patient 2 showed an increase in both WBC and RBC counts with a slightly reduced hemoglobin level. Repeat bone marrow biopsy in this patient showed decreased cellularity (50% as compared with 100% on the initial biopsy)

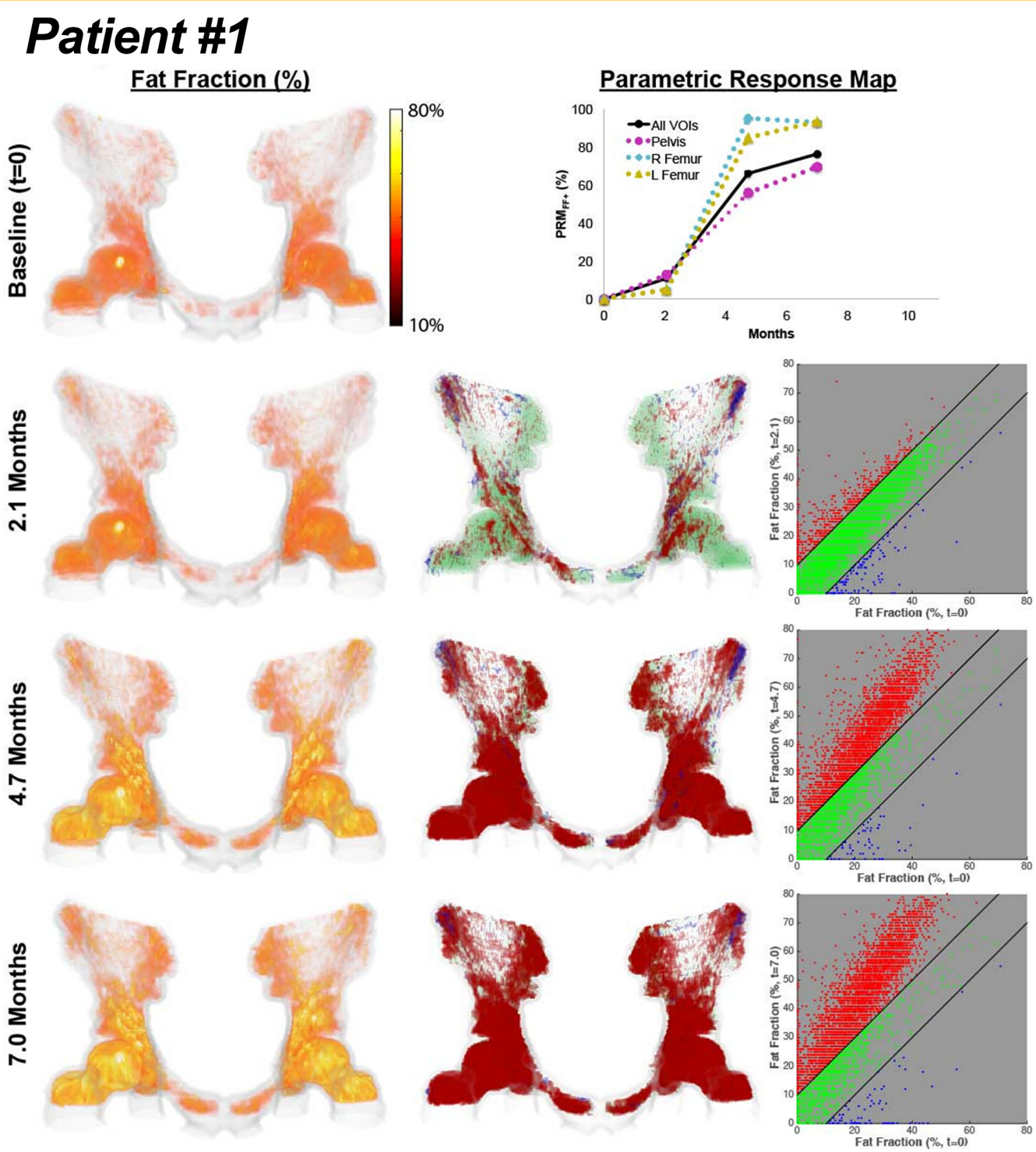

Figure 2. FF% and PRM analysis of changes in the bone marrow fat for patient 1. FF% in the pelvis and proximal femur measured by MRI at baseline and after 2.1, 4.7, and 7 months of treatment with ruxolitinib. Quantified FF% is displayed as a pseudocolor scale between 10% and 80% as shown on the scale bar. We present PRM data comparing post-treatment studies to the baseline MRI as an anatomic display, scatterplot, and line graph. On anatomic display and scatterplots, red denotes a significant increase in the bone marrow fat percentage; green represents no change; and blue designates a significant decrease. Readers can visualize a 4-dimensional (4D) display of the anatomic PRM display over the course of therapy for patient 1 (See Supplemental Video 1 PLAY VIDEO). Solid lines on scatterplots define the threshold for defining a significant change in MRI data for FF. The line plot shows time-course PRM_{FF+} readouts for the pelvis, each femur, and all three VOIs combined, as noted here.

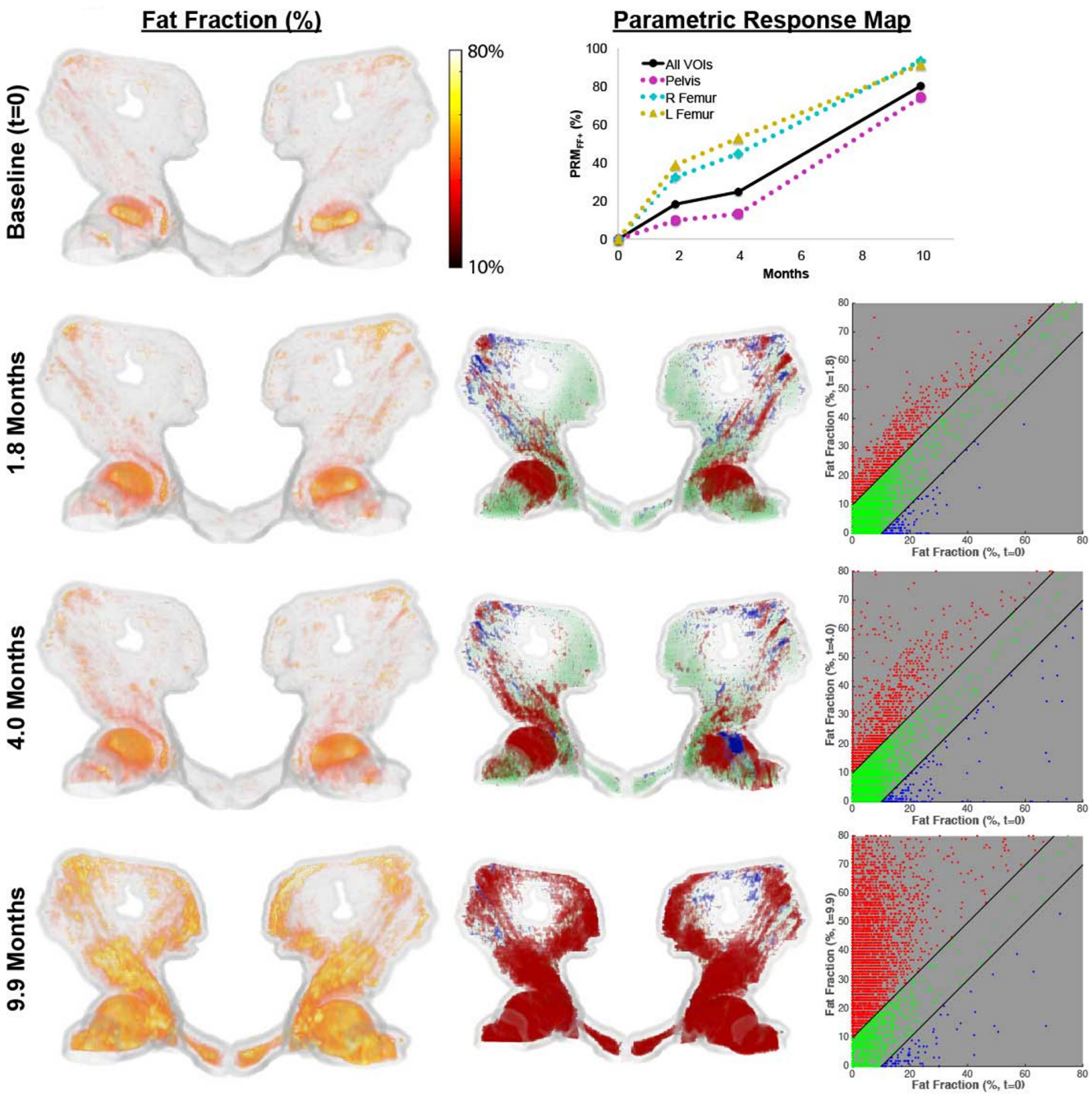

Figure 3. Analyzed imaging data for patient 2. FF% in the pelvis and proximal femur measured by MRI at baseline and after 1.8, 4, and 9.9 months of treatment with ruxolitinib. Quantified FF% and PRM results are displayed as described in Figure 2. Readers can visualize a 4D display of the anatomic PRM display over the course of therapy for patient 2 (See Supplemental Video 2 PLAY VIDEO).

with essentially constant fibrosis. The WBC count and other blood count parameters normalized after 8 months of treatment (Table 1).

Patient 3. Patient 3 had a preceding diagnosis of PV with a hypercellular (100%) bone marrow before therapy. Correspondingly, the pretreatment MRI showed very minimal fat within the bone marrow of the pelvis and proximal femurs because of replacement with hematopoietic cells (Figure 4). Over the course of the therapy, this patient showed almost no change in the bone marrow FF, with only a slight increase observed in both femoral heads. The PRM anatomic displays also revealed a loss of the bone marrow fat in both acetabula. Minimal increases in the bone marrow fat in the iliac bones and superior pubic rami after ~1 and 3 months were not apparent on the 6-month examina-

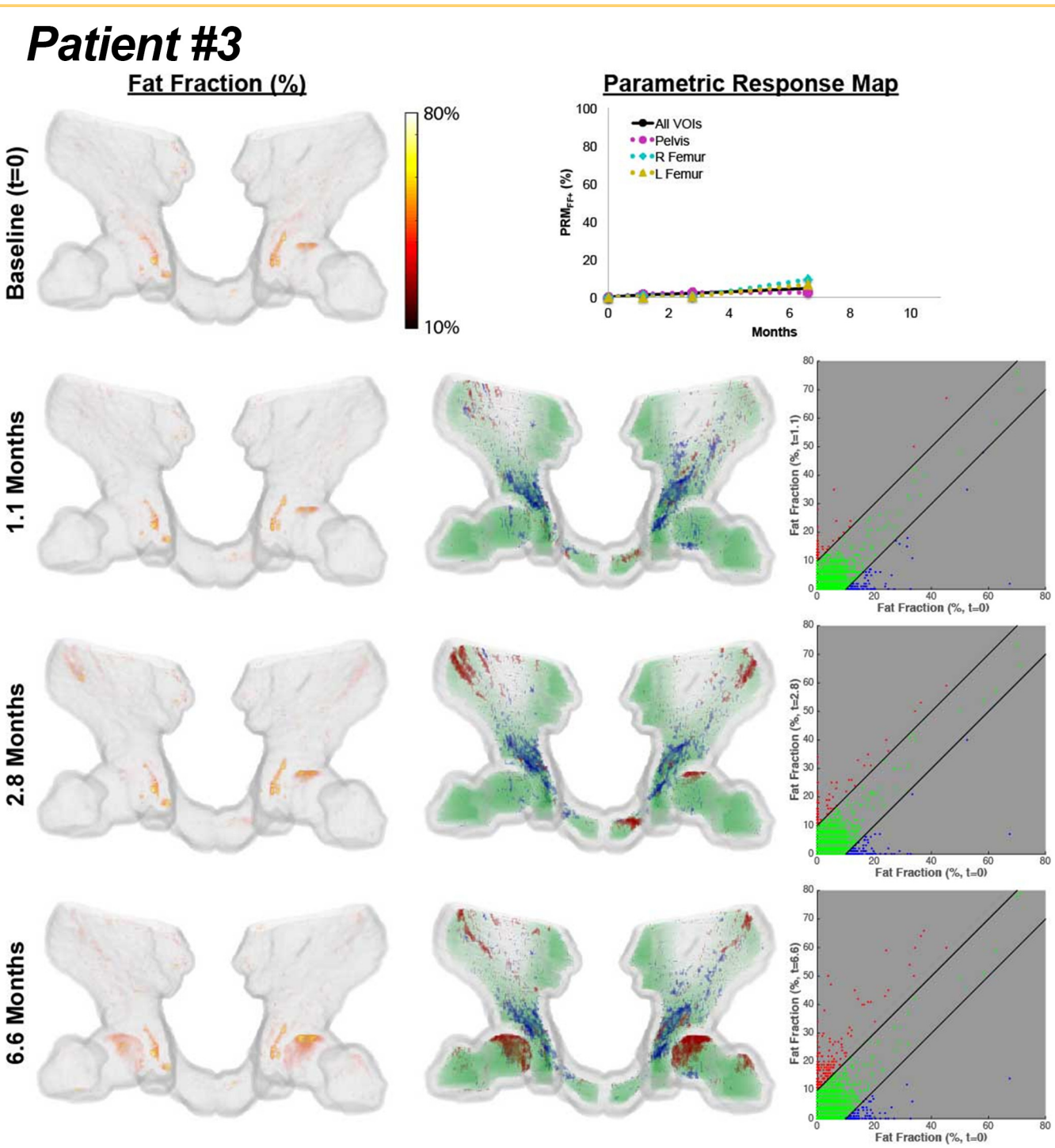

Figure 4. Analyzed imaging data for patient 3. FF% in the pelvis and proximal femur measured by MRI at baseline and after 1.1, 2.8, and 6.6 months of treatment with ruxolitinib. Quantified FF% and PRM results are displayed as described in Figure 2. Readers can visualize a 4D display of the anatomic PRM display over the course of therapy for patient 3 (See Supplemental Video 3 PLAY VIDEO).

tion. The PRM scatterplot also depicts the minimal fat content in the imaged bone marrow, with voxels confined to the origin. A 3D view of spatial and temporal changes in the PRM for this patient is included in Figure 4 legend. By comparison, spleen volume decreased by >30% over 6 months of therapy, nearly reaching the 35% threshold that is used as the standard imaging metric of treatment efficacy (Figure 6). The patient's elevated WBC count decreased to nearly normal levels by the end of treatment. Because this patient continued to have a PV phenotype requiring phlebotomy, the hemoglobin level and hemato-

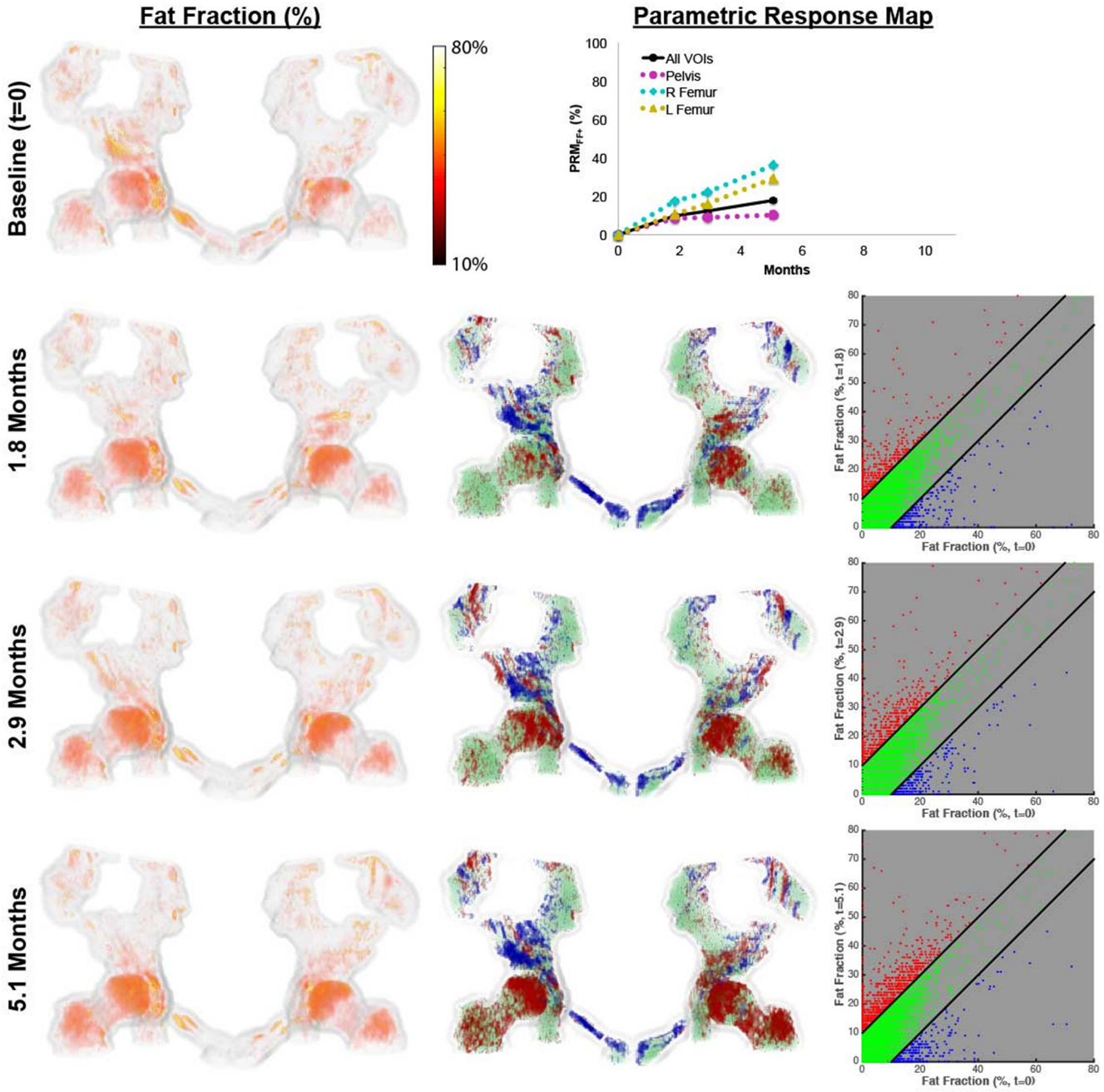

Figure 5. Analyzed imaging data for patient 4. FF% in the pelvis and proximal femur measured by MRI at baseline and after 1.8, 2.9, and 5.1 months of treatment with ruxolitinib. Quantified FF% and PRM results are displayed as described in Figure 2. Readers can visualize a 4D display of the anatomic PRM display over the course of therapy for patient 4 (See Supplemental Video 4 PLAY VIDEO).

crit values are reflective of intermittent phlebotomy to maintain hematocrit values to <45 (Table 1).

Patient 4. Patient 4 had MF secondary to PV, with a pretreatment bone marrow biopsy revealing densely fibrotic bone marrow (MF grade 3) and hypercellularity (60%; Table 1). The baseline image of the bone marrow FF shows ~40% fat predominantly in both femoral heads, with additional scattered foci of detectable fat throughout the pelvis (Figure 5). The FF maps show minimal changes in this distribution over the treatment course, with detectable increases in both femoral heads and loss of FF in the acetabula (right > left). The PRM anatomic color displays and scatterplots clearly depict marked heterogeneity of responses to treatment. The treatment increased the bone marrow fat in both femoral heads and proximal femurs, whereas fat

Table 1. Patient Demographics and Selected Laboratory Values

Patient	Age (y), Sex	MF Grade		Preceding Disease	WBC (K/μL) RBC Count (M/μL), Hemoglobin (g/dL), Hematocrit (%), and Platelets (K/μL)	
		Baseline	Treatment		*Baseline	*Treatment
1	63, M	2–3 (90% cellularity)	3 (40%–50% cellularity, high megakaryocytes)	Essential thrombocythemia	12.1 ↑	3.5 ↓
					4.44	2.98 ↓
					13.1 ↓	8.5 ↓
					41.2	25.7 ↓
					288	172
2	62, M	1 with limited 2 (hypercellular; 100%)	2 (variable with average 50% cellularity)	Polycythemia vera	20.6 ↑	8.9
					6.86 ↑	5.27
					13.4 ↓	15.1
					46.7	44.0
					335	178
3	51, M	1–2 (hypercellular, 100%)	NA	Polycythemia vera	18.8 ↑	10.8 ↑
					6.78 ↑	7.09 ↑
					13.2 ↓	12.9 ↓
					48.3	44.0**
					208	238
4	59, F	3 (60% cellularity)	NA	Polycythemia vera	8.7	7.0
					4.73	3.95
					11.2 ↓	9.7 ↓
					35.6 ↓	30.3 ↓
					101 ↓	86 ↓

* Normal values provided for comparison:
Normal (male):
WBC count: 4.0–10.0 k/μL.
RBC count: 4.40-5.70 M/uL.
Hemoglobin level: 13.5–17.0 g/dL.
Hematocrit value: 40.0%–50.0%.
Platelet count: 150–400 k/μL.
Normal (female):
WBC count: 4.0–10.0 k/μL.
RBC count: 3.9–5.0 M/uL.
Hemoglobin level: 12.0–16.0 g/dL.
Hematocrit value: 36%–48%.
Platelet count: 150-400 k/μL.
** Patient 3 still exhibited a polycythemia vera (PV) phenotype with intermittent polycythemia, so he underwent periodic phlebotomy to keep hematocrit value <45. Therefore, the hemoglobin level and hematocrit values are artificial.

decreased in both pubic rami and particularly the right acetabulum. Spatial and temporal changes in the PRM for patient 4 can be viewed in 4 dimensions via a link in Figure 5 legend. PRM data graphs show greater increases in fat in both femurs relative to the pelvis.

Anatomic imaging showed that spleen volume decreased by 35% in this patient over ~5 months of treatment (Figure 6), which meets the existing clinical imaging standard for response to ruxolitinib. WBC and RBC counts were normal both before and after therapy, although both values decreased slightly toward the lower range of normal. Hemoglobin level, hematocrit values, and platelet count were all below the normal range before treatment and remained below normal after 5 months of therapy; however, all these parameters decreased slightly with treatment (Table 1).

DISCUSSION

Although established clinical and pathologic staging systems define prognosis for patients with MF, monitoring the response to therapy remains an unmet clinical need in this disease. Because marked splenomegaly from extramedullary hematopoiesis is a hallmark feature of MF, reductions in spleen volume determined by either anatomic MRI or physical examination are standard metrics for treatment efficacy in MF. However, changes in spleen volume only indirectly assess the bone marrow fibrosis and do not predict durable responses to ruxolitinib or other drugs used for treating MF. A biopsy directly samples the bone marrow environment, but a blind biopsy of a single site

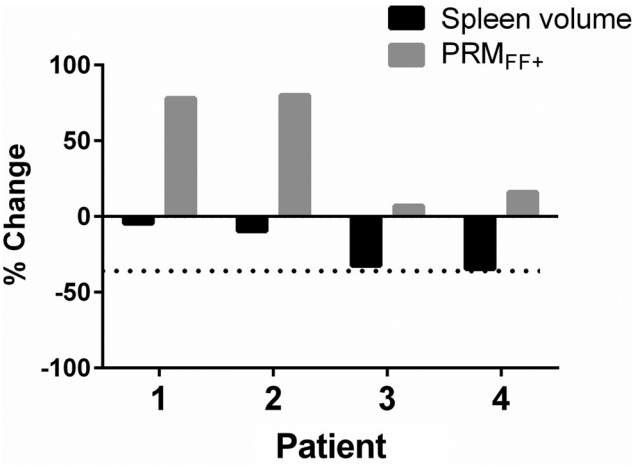

Figure 6. Changes in spleen volume from MRI. Percent decrease in spleen volume (black) is shown against the final PRM_{FF+} value (gray) for all 4 patients. The dashed line depicts a 35% reduction in spleen volume, which has been used as the primary clinical endpoint to define successful response to treatment with ruxolitinib (5). The PRM analysis shows substantial FF increases in patients 1 and 2 with minimal changes in patients 3 and 4. For each patient, the magnitude in the change for spleen volume and FF are, in general, inversely related.

in the iliac crest fails to account for heterogeneity of disease extent and treatment response throughout the skeleton. Bone marrow biopsy is also an invasive, uncomfortable procedure, limiting the frequency with which it is typically performed on a single patient in clinical practice. In addition, peripheral blood counts have limitations for assessing treatment response, in part, because off-target inhibition of the related kinase JAK1 can impair erythropoiesis (22).

The MRI method described in this study establishes the framework for a noninvasive, quantitative imaging test to more globally asses the bone marrow environment in patients with MF and monitor effects of therapy. The Dixon quantitative imaging technique we used to previously determine the fraction of the bone marrow fat has been shown to generate highly reproducible measurements in human subjects (23). MRI with the Dixon technique can detect increases in the bone marrow fat following systemic cancer chemotherapy or localized radiation therapy, a known complication of these treatments (24, 25). These data validate the Dixon technique for monitoring longitudinal changes in the bone marrow composition during therapy. Because vendors of clinical MRI scanners provide software for quantitative Dixon scan techniques, this imaging method can be implemented broadly in clinical research and patient care.

To track spatial and temporal changes in the bone marrow fat during therapy with ruxolitinib, we used PRM, a voxel-wise image analysis technique that quantifies and displays spatially varying alterations in FF longitudinally between pre- and post-treatment imaging examinations. Although PRM has been broadly used for imaging of cancer therapeutic response and other clinical diagnostic purposes, this study marks the first application of PRM for fat imaging and the bone marrow environment imaging (13, 26-42). In addition to the quantitative PRM metrics that condense response readouts into numerical values, a display of the PRM map allows for individual assessment of the spatial distribution of response. In the assessment of heterogeneous disease, the spatial context of response metrics is critical, particularly when evaluating against spatially limited readouts such as biopsies. Relative to images displaying the FF percent, the PRM color display enhanced conspicuity of regions with either increased or decreased bone marrow fat over the course of treatment. The PRM displays and associated graphs also provide quantitative metrics for voxels with changes in FF that exceed established confidence intervals for variability between MRI studies. The combination of quantitative Dixon MRI and PRM provides a powerful new approach to detect and quantify spatially heterogeneous changes in the bone marrow composition during therapy.

Our initial imaging results for patients with MF treated with ruxolitinib over ~5–10 months reveal several new, provocative observations. We observed substantial heterogeneity of responses among patients, with 2 patients (1 and 2) showing a pronounced increase in the bone marrow fat throughout the pelvis and proximal femurs, whereas another patient (3) had essentially no change in the bone marrow FF. Within a single patient, we identified heterogeneous responses of the marrow in different bones and even within the same bone. For example, the PRM of acetabula in patient 4 showed increased and decreased bone marrow fat in almost immediately adjacent voxels. In general, we also found that bone marrow FF increased to a greater extent in femurs relative to the pelvis. Finally, we observed a striking disconnect between effects of ruxolitinib on bone marrow FF versus spleen volume. Patient 1, with the most pronounced increase in bone marrow fat, had <5% reduction in spleen volume (Figure 6), the standard imaging parameter used for treatment efficacy. By comparison, patient 3 had negligible increases in bone marrow FF in the femur or pelvis but had >30% reduction in spleen volume (Figure 6). We are currently continuing to accrue additional patients into this study to correlate imaging data with clinical parameters and outcomes. Additional data from these patients will help to further elucidate how quantitative analysis of the bone marrow fat by MRI integrates with the current clinical metrics and potentially expands capabilities for assessing disease status for patient care.

Our study builds on a limited number of promising research for applications of MRI to MF. In clinical trials, measurements of spleen volume by anatomic MRI have been used to define response to therapy, with some trials using >35% reduction as the primary endpoint (5). Although bone marrow imaging has not been used to measure drug efficacy in MF, standard MRI techniques have been used to detect bone marrow abnormalities in patients with this disease. In a study of 35 patients with MF treated with hematopoietic stem cell transplant, qualitative evaluation of T1-weighted and short tau inversion recovery

images showed good correlation with the results of bone marrow biopsies (43). Resolution of bone marrow fibrosis and osteosclerosis by MRI also correlated with successful outcomes of stem cell transplants. In addition, dynamic contrast-enhanced MRI of the lumbosacral spine distinguished patients with MF from those with PV and ET on the basis of greater perfusion of bone marrow in patients with MF, which was attributed to neoangiogenesis (44).

Although the current study establishes feasibility of using quantitative MRI to analyze the bone marrow response to therapy in MF, technical improvements are needed to improve the use of this technique for clinical trials and possible patient management. Because test–retest imaging data were not available, a true assessment of the 95% confidence interval could not be used for the PRM threshold. This threshold will account for variation in the quantitative readout including image and Dixon modeling noise, image coregistration, and voxel geometry. Limitations in the spatial resolution of acquired images are problematic for delineation and analysis of narrow regions of interest, including the marrow space of the ilium, which is why the display for some patients (2 and 4, in Figures 3 and 5, respectively) appears to have a hole in the VOI. The data analysis methods used for this research required manual segmentation of bones on the baseline MRI as part of the PRM, which is a time-intensive process. Adding a high-resolution MRI sequence to define osseous anatomy, such as ultrashort echo time MRI, could alleviate this problem in future studies by facilitating automated segmentation and streamline data analysis.

MF is one of the most active areas of drug development in hematological malignancies, with several promising new treatments in preclinical development or clinical trials. These agents include inhibitors of telomerase, hedgehog signaling, and other compounds targeting JAK2 (45, 46), as well as antifibrotics that aim to reduce the bone marrow fibrosis. Quantitative imaging of the bone marrow fat with PRM to analyze spatial and temporal changes in FF has the potential to provide a more comprehensive assessment of treatment efficacy for clinical trials. This research establishes the feasibility of the MRI method for analyzing the bone marrow fat. Plans are underway to include this research as an exploratory endpoint in upcoming clinical trials with investigational agents. These and related studies will help determine to what extent quantitative MRI for bone marrow FF with PRM analysis will serve as an imaging biomarker for treatment efficacy in MF.

Supplemental Materials

Video 1: http://dx.doi.org/10.18383/j.tom.2016.00115.vid.01
Video 2: http://dx.doi.org/10.18383/j.tom.2016.00115.vid.02
Video 3: http://dx.doi.org/10.18383/j.tom.2016.00115.vid.03
Video 4: http://dx.doi.org/10.18383/j.tom.2016.00115.vid.04

ACKNOWLEDGMENTS

Gary D. Luker and Huong (Marie) Nguyen contributed equally to this work; and Brian D. Ross contributed equally as the corresponding author.

This research was supported by R01CA195655, R01CA170198, and R35CA197701.

Conflict of Interest: CJG, BDR, and TLC are inventors on patents related to the underlying technology, which have been exclusively licensed from the University of Michigan to Imbio, LLC, and thus may receive royalties. BDR also has shares in Imbio.

REFERENCES

1. Barosi G, Viarengo G, Pecci A, Rosti V, Piaggio G, Marchetti M, Frassoni F. Diagnostic and clinical relevance of the number of circulating CD34+ cells in myelofibrosis with myeloid metaplasia. Blood. 2001;98(12):3249–3255.
2. Cervantes F, Dupriez B, Pereira A, Passamonti F, Reilly JT, Morra E, Vannucchi AM, Mesa RA, Demory JL, Barosi G, Rumi E, Tefferi A. New prognostic scoring system for primary myelofibrosis based on a study of the International Working Group for Myelofibrosis Research and Treatment. Blood. 2009;113(3):2895–2901.
3. Cervantes F, Tassies D, Salgado C, Rovira M, Pereira A, Rozman C. Acute transformation in nonleukemic chronic myeloproliferative disorders: actuarial probability and main characteristics in a series of 218 patients. Acta Haematol. 1991;85(3):124–127.
4. Kiladjian JJ. The spectrum of JAK2-positive myeloproliferative neoplasms. Hematology Am Soc Hematol Educ Program. 2012;2012:561–566.
5. Verstovsek S, Mesa RA, Gotlib J, Levy RS, Gupta V, DiPersio JF, Catalano JV, Deininger M, Miller C, Silver RT, Talpaz M, Winton EF, Harvey JH Jr, Arcasoy MO, Hexner E, Lyons RM, Paquette R, Raza A, Vaddi K, Erickson-Viitanen S, Koumenis IL, Sun W, Sandor V, Kantarjian HM. A double-blind, placebo-controlled trial of ruxolitinib for myelofibrosis. N Engl J Med. 2012;366(9):799–807.
6. Deininger M, Radich J, Burn TC, Huber R, Paranagama D, Verstovsek S. The effect of long-term ruxolitinib treatment on JAK2p.V617F allele burden in patients with myelofibrosis. Blood. 2015;126(13):1551–1554.
7. Guglielmelli B, Biamonte F, Rotunno G, Artusi V, Artuso L, Bernardis I, Tenedini E, Pieri L, Paoli C, Mannarelli C, Fjerza R, Rumi E, Stalbovskaya V, Squires M, Cazzola M, Manfredini R, Harrison C, Tagliafico E, Vannucchi AM; COMFORT-II Investigators; Associazione Italiana per la Ricerca sul Cancro Gruppo Italiano Malattie Mieloproliferative (AGIMM) Investigators. Impact of mutational status on outcomes in myelofibrosis patients treated with ruxolitinib in the COMFORT-II study. Blood. 2014;123(14):2157–2160.
8. Koppikar P, Bhagwat N, Kilpivaara O, Manshouri T, Adli M, Hricik T, Liu F, Saunders LM, Mullally A, Abdel-Wahab O, Leung L, Weinstein A, Marubayashi S, Goel A, Gönen M, Estrov Z, Ebert BL, Chiosis G, Nimer SD, Bernstein BE, Verstovsek S, Levine RL. Heterodimeric JAK-STAT activation as a mechanism of persistence to JAK2 inhibitor therapy. Nature. 2012;489(7414):155–159.
9. Gangat N, Caramaza D, Vaidya R, Gerorge G, Begna K, Schwager S, Van Dyke D, Hanson C, Wu W, Pardanani A, Cervantes F, Passamonti F, Tefferi A. DIPSS plus: a refined Dynamic International Prognostic Scoring System for primary myelofibrosis that incorporates prognostic information from karyotype, platelet count, and transfusion status. J Clin Oncol. 2011;29(4):392–397.
10. Thiele J, Kvasnicka HM, Facchetti F, Franco V, van der Walt J, Orazi A. European consensus on grading bone marrow fibrosis and assessment of cellularity. Haematologica. 2005;90(8):1128–1132.
11. Gianelli U, Vener C, Bossi A, Cortinovis I, Iurlo A, Fracchiolla NS, Savi F, Moro A, Grifoni F, De Philippis C, Radice T, Bosari S, Lambertenghi Deliliers G, Cortelezzi A. The European Consensus on grading of bone marrow fibrosis allows a better prognostication of patients with primary myelofibrosis. Mod Pathol. 2012;25(9):1193–1202.
12. Tuliapurkar SR, McGuire TR, Brusnahan SK, Jackson JD, Garvin KL, Kessinger MA, Lane JT, O' Kane BJ, Sharp JG. Changes in human bone marrow fat content associated with changes in hematopoietic stem cell numbers and cytokine levels with aging. J Anat. 2011;19(5):574–581.
13. Galbán CJ, Chenevert TL, Meyer CR, Tsien C, Lawrence TS, Hamstra DA, Junck L, Sundgren PC, Johnson TD, Ross DJ, Rehemtulla A, Ross BD. The parametric response map: an imaging biomarker for early cancer treatment outcome. Nat Med. 2009;15(5):572–576.
14. Moffat BA, Chenevert TL, Meyer CR, McKeever PE, Hall DE, Hoff BA, Johnson TD, Rehemtulla A, Ross BD. The functional diffusion map: an imaging biomarker for the early prediction of cancer treatment outcome. Neoplasia. 2006;8(4):259–267.

15. Reischauer C, Koh DM, Froehlich JM, Patzwahi R, Binkert CA, Gutzeit A. Pilot study on the detection of antiandrogen resistance using serial diffusion-weighted imaging of bone metastases in prostate cancer. J Magn Reson Imaging. 2015; Nov 20. doi: 10.1002/jmri.25102 [Epub ahead of print].
16. Reischauer C, Froehlich JM, Koh DM, Graf N, Padevit C, John H, Binkert CA, Boesiger P, Gutzeit A. Bone metastases from prostate cancer: assessing treatment response by using diffusion-weighted imaging and functional diffusion maps–initial observations. Radiology. 2010;257(2):523–531.
17. Hernando D, Haldar JP, Sutton BP, Ma J, Kellman P, Liang ZP. Joint estimation of water/fat images and field inhomogeneity map. Magn Reson Med. 2008;59(3): 571–580.
18. Hussain HK, Chenevert TL, Londy FJ, Gulani V, Swanson SD, Mckenna BJ, Appelman HD, Adusumilli S, Greenson JK, Conjeevaram HS. Hepatic fat fraction: MR imaging for quantitative measurement and display–early experience. Radiology. 2005;237(3):1048–1055.
19. Hines CD, Yu H, Shimakawa A, McKenzie CA, Brittain JH, Reeder SB. T1 independent, T2* corrected MRI with accurate spectral modeling for quantification of fat: validation in a fat-water-SPIO phantom. J Magn Reson Imaging. 2009;30(5): 1215–1222.
20. Hernando D, Bashir M, Hamilton G, Shaffer J, Sharma S, Sirlin C, Sofue K, Szeverenyi NM, Yokoo T, Yuan Q, Reeder SB. Multi-site, multi-vendor validation of accuracy, robustness and reproducibility of fat quantification on an oil-water phantom at 1.5T and 3T. ISMRM. 2015; Milan, Italy.
21. Klein S, Staring M, Murphy K, Viergever MA, Pluim JP. elastix: a toolbox for intensity-based medical image registration. IEEE Trans Med Imaging. 2010;29(1): 196–205.
22. Tefferi A. JAK inhibitors for myeloproliferative neoplasms: clarifying facts from myths. Blood. 2012;119(12):2721–2730.
23. Maas M, Akkerman EM, Venema HW, Stoker J, Den Heeten GJ. Dixon quantitative chemical shift MRI for bone marrow evaluation in the lumbar spine: a reproducibility study in healthy volunteers. J Comput Assist Tomogr. 2001;25(5):691–697.
24. Bolan PJ, Arentsen L, Sueblinvong T, Zhang Y, Moeller S, Carter JS, Downs LS, Ghebre R, Yee D, Froelich J, Hui S. Water–fat MRI for assessing changes in bone marrow composition due to radiation and chemotherapy in gynecologic cancer patients. J Magn Reson Imaging. 2013;38(6):1578–1584.
25. Carmona R, Pritz J, Bydder M, Gulaya S, Zhu H, Williamson CW, Welch CS, Vaida F, Bydder G, Mell LK. Fat composition changes in bone marrow during chemotherapy and radiation therapy. Int J Radiat Oncol Biol Phys. 2014;90(1): 155–163.
26. Boes JL, Hoff BA, Bule M, Johnson TD, Rehemtulla A, Chamberlain R, Hoffman EA, Kazerooni EA, Martinez FJ, Han MK, Ross BD, Galbán CJ. Parametric response mapping monitors temporal changes on lung CT scans in the subpopulations and intermediate outcome measures in COPD Study (SPIROMICS). Acad Radiol. 2015;22(2):186–194.
27. Ellingson BM, Malkin MG, Rand SD, Connelly JM, Quinsey C, LaViolette PS, Bedekar DP, Schmainda KM. Validation of functional diffusion maps (fDMs) as a biomarker for human glioma cellularity. J Magn Reson Imaging. 2010;31(3): 538–548.
28. Galbán CJ, Lemasson B, Hoff BA, Johnson TD, Sundgren PC, Tsien C, Chenevert TL, Ross BD. Development of a multiparametric voxel-based magnetic resonance imaging biomarker for early cancer therapeutic response assessment. Tomography. 2015;1(1):44–52.
29. Harris RJ, Cloughesy TF, Pope WB, Nghiemphu PL, Lai A, Zaw T, Czernin J, Phelps ME, Chen W, Ellingson BM. 18F-FDOPA and 18F-FLT positron emission tomography parametric response maps predict response in recurrent malignant gliomas treated with bevacizumab. Neuro Oncol. 2012;14(8):1079–1089.
30. Brisset JC, Hoff BA, Chenevert TL, Jacobson JA, Boes JL, Galbán S, Rehemtulla A, Johnson TD, Pienta KJ, Galbán CJ, Meyer CR, Schakel T, Nicolay K, Alva AS, Hussain M, Ross BD. Integrated multimodal imaging of dynamic bone-tumor alterations associated with metastatic prostate cancer. PLoS One. 2015;10(4): e0123877.
31. Galbán CJ, Ma B, Malyarenko D, Pickles MD, Heist K, Henry NL, Schott AF, Neal CH, Hylton NM, Rehemtulla A, Johnson TD, Meyer CR, Chenevert TL, Turnbull LW, Ross BD. Multi-site clinical evaluation of DW-MRI as a treatment response metric for breast cancer patients undergoing neoadjuvant chemotherapy. PLoS One. 2015;10(3):e0122151.
32. Ruiz-Espana S, Jimenez-Moya A, Arana E, Moratal D. Functional diffusion map: A biomarker of brain metastases response to treatment based on magnetic resonance image analysis. Conf Proc IEEE Med Biol Soc. 2015;2015:4282–4285.
33. Ellingson BM, Kim E, Woodworth DC, Marques H, Boxerman JL, Safriel Y, McKinstry RC, Bokstein F, Jain R, Chi TL, Sorensen AG, Gilbert MR, Barboriak DP. Diffusion MRI quality control and functional diffusion map results in ACRIN 6677/RTOG 0625: a multicenter, randomized, phase II trial of bevacizumab and chemotherapy in recurrent glioblastoma. Int J Oncol. 2015;46(5):1883–1892.
34. Lemasson B, Galbán CJ, Boes JL, Li Y, Zhu Y, Heist KA, Johnson TD, Chenevert TL, Galbán S, Rehemtulla A, Ross BD. Diffusion-weighted MRI as a biomarker of tumor radiation treatment response heterogeneity: a comparative study of whole-volume histogram analysis versus voxel-based functional diffusion map analysis. Transl Oncol. 2013;6(5):554–561.
35. Galbán CJ, Mukherji SK, Chenevert TL, Meyer CR, Hamstra DA, Bland PH, Johnson TD, Moffat BA, Rehemtulla A, Eisbruch A, Ross BD. A feasibility study of parametric response map analysis of diffusion-weighted magnetic resonance imaging scans of head and neck cancer patients for providing early detection of therapeutic efficacy. Transl Oncol. 2009;2(3):184–190.
36. Lee KC, Sud S, Meyer CR, Moffat BA, Chenevert TL, Rehemtulla A, Pienta KJ, Ross BD. An imaging biomarker of early treatment response in prostate cancer that has metastasized to the bone. Cancer Res. 2007;67:3524–3528.
37. Moffat BA, Chenevert TL, Lawrence TS, Meyer CR, Johnson TD, Dong Q, Tsien C, Mukherji S, Quint DJ, Gebarski SS, Robertson PL, Junck LR, Rehemtulla A, Ross BD. Functional diffusion map: a noninvasive MRI biomarker for early stratification of clinical brain tumor response. Proc Natl Acad Sci U S A. 2005;102(15): 5524–5529.
38. Hamstra DA, Chenevert TL, Moffat BA, Johnson TD, Meyer CR, Mukherji SK, Quint DJ, Gebarski SS, Fan X, Tsien CI, Lawrence TS, Junck L, Rehemtulla A, Ross BD. Evaluation of the functional diffusion map as an early biomarker of time-to-progression and overall survival in high-grade glioma. Proc Natl Acad Sci U S A. 2005;102(46):16759–16764.
39. Hoff BA, Toole M, Yablon C, Ross BD, Luker GD, VanPoznak C, Galbán CJ. Potential for early fracture risk assessment in patients with metastatic bone disease using parametric response mapping of CT images. Tomography. 2015;1(2):98–104.
40. Boudewijn IM, Postma DS, Telenga ED, Ten Hacken NH, Timens W, Oudkerk M, Ross BD, Galbán CJ, van den Berge M. Effects of ageing and smoking on pulmonary computed tomography scans using parametric response mapping. Eur Respir J. 2015;46(4):1193–1196.
41. Capaldi D, Zha N, Guo F, Pike D, McCormack D, Kirby M, Parraga G. Pulmonary imaging biomarkers of gas trapping and emphysema in COPD: 3He MR imaging and CT parametric response maps. Radiology. 2016;151484 [Epub ahead of print].
42. Tsai YH, Hsu LM, Weng HH, Lee MH, Yang JT, Lin CP. Functional diffusion map as an imaging predictor of functional outcome in patients with primary intracerebral haemorrhage. Br J Radiol. 2013;86(1021):20110644.
43. Sale GE, Deeg HJ, Porter BA. Regression of myelofibrosis and osteosclerosis following hematopoietic cell transplantation assessed by magnetic resonance imaging and histologic grading. Biol Blood Marrow Transplant. 2006;12(12): 1285–1294.
44. Courcoutsakis N, Spanoudaki A, Maris TG, Astrinakis E, Spanoudakis E, Tsatalas C, Prassopoulos P. Perfusion parameters analysis of the vertebral bone marrow in patients with Ph^{1-} chronic myeloproliferative neoplasms (Ph(neg) MPN): a dynamic contrast-enhanced MRI (DCE-MRI) study. J Magn Reson Imaging. 2012; 55(3):696–702.
45. Odenike O. Beyond JAK inhibitor therapy in myelofibrosis. Hematology Am Soc Hematol Educ Program. 2013;2013(1):545–552.
46. Stein BL, Swords R, Hochhaus A, Giles F. Novel myelofibrosis treatment strategies: potential partners for combination therapies. Leukemia. 2014;28(11): 2139–2147.